Published in final edited form as:
Bone. 2012 August ; 51(2): 212–217. doi:10.1016/j.bone.2011.11.030.

Elevated cross-talk between subchondral bone and cartilage in osteoarthritic joints

Jun Pan[1,2,*], **Bin Wang**[1,2], **Wen Li**[2], **Xiaozhou Zhou**[2], **Thomas Scherr**[2], **Yunyi Yang**[2], **Christopher Price**[2], and **Liyun Wang**[2,*]

[1]Key Laboratory for Biorheological Science and Technology of Ministry of Education, Bioengineering College, Chongqing University, Chongqing 400044, PR China

[2]Center for Biomedical Engineering Research, Department of Mechanical Engineering, University of Delaware, Newark, DE 19716, USA

Abstract

Osteoarthritis (OA) is a degenerative joint disease and one of the leading causes of disability in the United States and all over the world. As a disease of the whole joint, OA exhibits a complicated etiology with risk factors including, but not limited to, ageing, altered joint loading, and injury. Subchondral bone is hypothesized to be involved in OA development. However, direct evidence supporting this is lacking. We previously detected measurable transport of solute across the mineralized calcified cartilage in normal joints, suggesting a potential cross-talk between subchondral bone and cartilage. Whether this cross-talk exists in OA has not been established yet. Using two models that induced OA by either ageing or surgery (destabilization of medial meniscus, DMM), we tested the hypothesis that increased cross-talk occurs in OA. We quantified the diffusivity of sodium fluorescein (376Da), a marker of small-sized signaling molecules, within calcified joint matrix using our newly developed fluorescence loss induced by photobleaching (FLIP) method. Tracer diffusivity was found to be 0.30±0.17 and 0.33±0.20 $\mu m^2/s$ within the calcified cartilage and 0.12±0.04 and 0.07±0.03 $\mu m^2/s$ across the osteochondral interface in the aged (20–24-month-old, n=4) and DMM OA joints (5-month-old, n=5), respectively, comparable to the values for the contralateral non-operated joints in the DMM mice (0.48±0.13 and 0.12±0.06 $\mu m^2/s$). Although we did not detect significant changes in tissue matrix permeability in OA joints, we found i) an increased number of vessels invading the calcified cartilage (and sometimes approaching the tidemark) in the aged (+100%) and DMM (+50%) joints relative to the normal age controls; and ii) a 60% thinning of the subchondral bone and calcified cartilage layers in the aged joints (with no significant changes detected in the DMM joints). These results suggested that the capacity for cross-talk between subchondral bone and articular cartilage could be elevated in OA. Further studies are needed to identify the direction of the cross-talk, the signaling molecules involved, and to test whether subchondral bone changes initiate OA development and could serve as a pharmaceutical target for OA treatment.

[*]Corresponding author: Liyun Wang, PhD., 302-831-2659 (voice), 302-83-3619 (fax); lywang@udel.edu, 130 Academy St, Spencer Lab 126, University of Delaware, Newark, DE 19716. Jun Pan, Key Laboratory for Biorheological Science and Technology of Ministry of Education, Bioengineering College, Chongqing University, Chongqing 400044, PR China. Fax: +86-23-65460031; panj@cqu.edu.cn.

Keywords

Calcified cartilage; Osteochondral interface; Permeability; Osteoarthritis; ageing; destabilized medial meniscus

Introduction

Osteoarthritis (OA), one of the leading causes of chronic disability in the United States and across the world [1], is a degenerative joint disease characterized by the loss of articular cartilage and abnormal changes in the surrounding soft and hard tissue of the joint, including bone. Currently, no effective treatment is available to cure OA due to its complex etiology and a lack of effective pharmaceutical targets [1]. Although many risk factors such as genetics, age, obesity, and altered joint loading have been identified in OA patients [1], the mechanisms for the initiation and progression of OA are not well understood. There is a growing consensus that OA is a whole-joint disease [2, 3]. In particular, increased turnover of subchondral bone found in OA patients and animal models [4, 5] has led to the hypothesis that the various cytokines and growth factors released during subchondral bone turnover may reach the overlying articular cartilage and initiate a vigorous positive feedback loop between the attempted cartilage and bone repair processes that eventually leads to OA progression [6]. Recent experimental data support this hypothesis. For example, administration of osteoprotegerin prevented not only trabecular bone loss but also cartilage degradation in a surgically induced OA model [7]. The aggrecanase-2 deficient (ADAMTS5−/−) mice, which were found to be protected from cartilage degeneration after joint instability, showed less severe subchondral bone changes compared to the wild type controls [8]. At the cellular level, osteoblasts from OA patients induced hypertrophic differentiation and matrix mineralization of normal chondrocytes *in vitro* [9]. Despite this indirect evidence, direct crosstalk between the subchondral bone and articular cartilage has not been established in OA joints.

Recently we demonstrated the potential for cross-talk between subchondral bone and articular cartilage in normal mature joints [10]. By using an advanced imaging approach based on fluorescence loss induced by photobleaching (FLIP), we quantified the permeability of calcified cartilage and the osteochondral interface to a small molecular-weight tracer (sodium fluorescein, 376Da) in the knee joints of adult mice. Our results, of measurable solute transport across the joints, challenged the long held view that the calcified cartilage separating the subchondral bone and articular cartilage is impermeable [11–13]. With OA, alterations in the structural and material properties of joint tissues have been reported [8, 14–17]. In addition, vascular channels [18, 19] or microcracks [20, 21], which could act as transport conduits, have been reported in OA joints. How the matrix property and structural alterations of the OA joints translate to functional changes in bone-cartilage cross-talk is not clear.

In the present study, we quantified matrix permeability, vessel invasion, and overall joint morphology in two well-established OA models: age-related spontaneous OA [22], and altered loading (surgery) induced OA [23]. Our hypothesis was that the communication potential between subchondral bone and articular cartilage increases in OA. In this study, we first used FLIP to quantify the permeability of the calcified cartilage and the osteochondral interface, the main barrier for transport of molecular signals between the joint tissues (permeability on the order of 0.1–0.5 $\mu m^2/s$ [10], two to three orders of magnitude smaller than those of bone and articular cartilage) [24, 25]. We then measured the overall joint morphology and the number density of invading vessels using confocal microscopy. When compared to controls it was observed that OA was not associated with significant changes in

tissue matrix permeability in either OA model. However, OA did result in an increase in the blood vessels that invaded (and perforated) the calcified cartilage in both models and also led to a thinning of the subchondral bone and calcified cartilage layers in the aged joints. Together, these results suggested that the capacity for cross-talk between subchondral bone and articular cartilage could be elevated in OA due to morphological alterations in the joint.

Materials and Methods

Experimental groups

Two murine OA models were utilized within this study. The first was the age-related spontaneous OA model in which C57BL/6J mice (n=13) were aged until twenty to twenty-four months of age, at which time mild-to-moderate bi-lateral knee OA is observed as previously described in the literature [22]. The second model was the surgical destabilization of the medical meniscus (DMM) OA model [23]. In this portion of the study male C57BL/6J mice (n=14) were subjected to DMM surgery at the age of three-months as described previously [23]. Briefly, under aseptic conditions, the right knee joint capsule was opened, and the ligament attaching the medial meniscus to the tibia was transected to impair the stability of the joint structure [23]. The left joints were not operated and served as internal controls. The mice were sacrificed 8 weeks post surgery (at the age of five-months), and subjected to cartilage integrity (Safranin-O/Fast green staining) and matrix permeability examinations (FLIP measurements and basic fuchsin staining) as detailed below. In addition, ten separate five-month-old male C57BL/6J mice were used as controls for histological examination of cartilage damage and vessel invasions. These baseline control measurements were compared with those in aged mice (5-months vs. 20–24-months) or mice with altered knee loading conditions (intact vs. DMM joints). All mice were purchased from The Jackson Laboratory (The Jackson Laboratory, Bar Harbor, ME). The study was approved by the Institutional Animal Care and Use Committee.

To first validate our OA mice models, joint samples from a subset of aged, DMM, and control groups were examined using standard histology to evaluate cartilage damage following previously published procedures [23]. Briefly, joints from aged mice (right joints, n=5), DMM mice (both the operated right joints and the left contralateral joints, n=6), and control mice (right joints, n=6) were harvested, fixed in 10% neutral buffed formalin, and decalcified with formic acid before being embedded in paraffin. Sequential frontal sections (5 μm thick) were obtained using a microtome and collected onto positively charged glass slides (2–3 sections per slide). To assess damage through the entire joint, 12–15 slides covering the full thickness of the joint were chosen and stained with 0.1% Safranin O and Fast Green. The sections were blindly scored under light microscopy by two observers (JP, TS) within four compartments (medial and lateral femoral condyles; medial and lateral tibial plateaus), following a semi-quantitative grading scale [23], where 0 = normal cartilage; 0.5 = loss of Safranin-O with no structural lesions; 1 = roughened articular surface and small fibrillations; 2 = fibrillation below the superficial layer and some loss of lamina; 3 = fibrillations extending to the calcified cartilage across less than 25% of the cartilage width; 4 = fibrillations extending to the calcified cartilage across 25–50% of the cartilage width; 5 = fibrillation and erosions extending from 50 to 75% of the cartilage width; 6 = cartilage erosion extending beyond 75% of the cartilage width. The average score from all the sections was reported for each knee. The scores confirmed significant but mild cartilage damage in the aged and DMM groups compared with the normal controls (detailed in the Results section). Based upon this validation both of the OA models were utilized for the following quantitative studies.

Matrix permeability measurements using FLIP

To quantify the permeability of the calcified cartilage and of the osteochondral interface, a subset of DMM mice (n=5) and aged mice (n=4) were subjected to FLIP tests using our previously published procedures [10]. The operated and the contralateral joints from the DMM mice, as well as the right joints from the aged mice were utilized. No difference was found in the cartilage damage score between the DMM contralateral joints and the normal 5-month-old B6 joints, thus the contralateral joints served as undamaged (internal) controls for the DMM operated joints. Briefly, mice were injected with a bolus of sodium fluorescein solution (2mg in 0.5mL) via tail vein injection. After ~0.5 hour, the mice were sacrificed, and distal femurs were harvested immediately and sagittally split along the notch between the two condyles. After trimming the cut surface with a diamond knife in a cryostat, the halved samples were mounted on a cover glass, and imaged using an inverted confocal laser scanning microscope (Zeiss LSM 510; Standort Gőttingen, Germany). Individual chondrons within calcified cartilage and osteocyte lacunae near the osteochondral interface that were 5–20 μm below the cutting surface were readily identified based on their shapes (spherical vs. ellipsoidal) and size (20 vs. 10 microns). A single chondron (transport sink) was subjected to continuous photobleaching and the surrounding chondrons and/or osteocyte lacunae (transport sources) were monitored using a time series of confocal images as describe previously [10]. Sources and sinks were chosen based on 3D examination of the region of interest and the following criteria: 1) they were clearly observed during confocal imaging procedure with no drifting or movement artifacts; 2) there was no other cells located between the source and the sink that may interfere tracer transport; multiple sources could be chosen for the same sink; 3) the (edge-to-edge) spacing between the source-sink was in the range of 0.5–7 fold of the source radius and the sink/source size ratio was between 0.5–3, because correction factors accounting for these ranges of source-sink spacing and size ratio have been numerically obtained in our previous study [10]. Using our bispherical transport model [10], the effective diffusivity (D) of the tracer between the source and sink chondrons within the calcified cartilage (termed C-C) as well as between the source osteocytes and sink chondron across the osteochondral interface (termed O-C) was derived by curving fitting the experimental intensity data with the model. Typically, three to six FLIP experiments were performed per joint and two to four pairs of source-sink per FLIP experiment were fit with the model. Only the diffusivities from reasonable good curve fitting (R^2>= 0.80) were used. The average values of the C-C and O-C permeability were obtained from the repeated measures for each joint and used for comparisons between testing regions (C-C vs. O-C) for the DMM vs. contralateral joints, or young vs. aged joints.

Joint morphology and vessel invasions

The overall transport across the joint is dependent on not only the local ECM permeability (examined above) but also the structural features such as the thickness of each tissue layer and the number density of the large vascular channels perforating the ECM. Joint tissue thickness and vessel invasions were measured using three dimensional confocal imaging. The right distal femurs from normal age control, DMM, and aged groups (n=4 joints per group) were bulk stained with basic fuchsin, and embedded in plastics following a previously published protocol [26]. Sagittal sections of 200 μm thickness (6–7 sections per joint) were obtained using a diamond saw and surface polished before being mounted on glass slides. The sections were observed using the Zeiss LSM 510 confocal microscope with a 40x oil-immersion objective under an excitation and emission of 561/640 nm. Multiple z-stack images consisting of 6 slices with a 2μm interval were taken and stitched together to map the entire epiphysis of the distal femur. Due to the distinct cellular morphology and ECM staining patterns, different tissues can be readily identified (Fig. 1); as seen in the strong staining intensity and amorphous pattern for marrow cavities, the numerous canalicular channels and spindle-shaped osteocyte lacunae on a unstained matrix

background for subchondral bone (SB), the large rounded hypertrophic chondrons on an unstained matrix background for calcified cartilage (CC), as well as the continuous strong staining at the tidemark (TM) interface between calcified cartilage and articular cartilage (AC) (Fig. 1). Within the imaging stacks, it was relatively easy to trace and identify blood vessels or marrow cavities in three dimensions (defined as linear continuous features with >=10 microns in diameter/width), which might not be distinguishable from other cellular features in 2D histological sections. The number of blood vessels abutted to the SB, CC or TM layer was counted within the load-bearing portion of the femoral condyle using the Zeiss LSM software. The number density of the invading vessels ended at each layer was calculated in reference of the articular surface area, which was estimated by multiplying the tidemark length and the depth of the z-stack thickness (12 μm). The z-stack images were then exported to TIFF files and the outlines of AC, TM, CC, and SB were manually traced in the Adobe Photoshop software on a digitizing interactive pen display. The average thickness values for the tissue layers (SB, CC, AC) were obtained from the outlined regions of interest using a custom MatLab code. We also reported the total joint thickness by summation of the thicknesses of the three layers.

Statistical analysis

Descriptive data were presented as means and standard deviations. Statistical significance was determined using Student t tests (paired or unpaired) or one-way ANOVA with Bonferroni post hoc tests in the Origin software package. Statistical significance was defined as $p < 0.05$.

Results

Validation of the OA models

Compared with the normal age controls (n=6), higher scores were seen in most quadrants of the aged joints (except for lateral tibia, n=5) and in all four quadrants of the DMM joints (n=6, * indicates $p < 0.05$ in Fig. 2). Overall, the damage was mild (OA score less than 1.2 out of a full range of 6) for both the aged and the DMM joints (Fig. 2). The left unoperated joints in the DMM mice displayed negligible cartilage damage as the normal age controls (data not shown), and thus were used as control joints for the FLIP study. In sections from 5-month-old control mouse (Fig. 3A, representative image shown). Safranin-O/Fast Green staining demonstrated smooth undamaged articular surface in the medial femoral condyle (MF) and medial tibial plateau (MT). In sections from DMM joints (Fig. 3B, representative image shown), areas (indicated with black arrow heads) with a damage score of 3 (damage extending to the calcified cartilage across less than 25% of the cartilage width) and a damage score of 1 (roughened articular surface and small fibrillations) were readily observed in the MF and MT, respectively. In aged joints (Fig. 3C, representative image shown), these same regions demonstrated areas with damage scores of 1 and 2 (fibrillation below the superficial layer and some loss of lamina). Please note that the values shown for the four quadrants (medial and lateral femoral/tibial condyles) in Fig. 2 were averaged over more than ten sections spanning the entire joint. Although the knee medial compartments in the DMM joints were reported to have more severe damage than the lateral compartments when examined at longer time points post surgery in literature [23], such compartmental difference was not seen in our DMM mice 8 weeks post surgery.

Matrix permeability measurements using FLIP

A total of 42, 28, and 43 source-sink pairs for C-C measurements, and 23, 25, and 25 source-sink pairs for O-C measurements, which fit the model well (R^2>=0.8), were collected and analyzed for the DMM knees (n=5), their contralateral unoperated control knees (n=5), and the aged knees (n=4), respectively. Within the groups examined, the control knees of the

DMM mice (age of 5-months) showed four-fold increase in the mean diffusivity of sodium fluorescein measured between chondrons within calcified cartilage (C-C) than that measured between osteocytes and chondron (O-C) in the same joints ($p<0.05$; Table 1). A similar degree of permeability increase in C-C over O-C was found in the DMM operated joints of the same mice (2.5-fold) as well as the joints of much older mice (age of 20–24 months, 4.7-fold). These changes, however, did not reach statistical significance possibly due to small sample size. Eight weeks of altered joint loading resulted in a −37.5% decrease in the C-C permeability and no change in the O-C permeability in the DMM operated knees compared with the control knees ($p>0.05$, Table 1). Meanwhile, the aged knees (age of 20–24 months) showed −31.2% and −41.7% decrease in the C-C and O-C permeability, respectively, compared with the younger control knees ($p>0.05$, Table 1).

Joint morphology and vessel invasion

Compared with the normal age controls (n=4), the average thicknesses of the SB and CC layers and the total joint thickness were significantly reduced (−60%) in the aged group, while no significant difference was detected in any of the tissue layers in the DMM joints (Fig. 4). The number density of the vessels invading the CC layers showed 1 and 0.5-fold increase in the aged and DMM groups, respectively (Table 2). There were no vessel invading the tidemark in normal joints while vessels approached tidemark in the aged and DMM joints at a density of 51 and 18 per mm^2 (Table 2). Representative basic fuchsin images showed that blood vessels and marrow spaces advanced closer to articular cartilage in joints subjected to altered loading (Fig. 1B) and in aged joints (Fig. 1C), compared with normal aged joints without altered loading (control, Fig. 1A).

Discussion

Recent evidence suggests that subchondral bone may be involved in OA development and that bone and cartilage are functionally coupled through either the distribution of joint loads or by exchanging signaling molecules between the two adjacent tissues [2, 15, 17, 27]. However, the transport pathways for the cross-talk between these two tissues are not fully understood. Combining animal models, advanced imaging, and mathematical modeling, the present work demonstrated that the capacity for communicating biochemical signals between the subchondral bone and cartilage was greatly increased in both altered loading (DMM) and ageing induced OA models, with apparently different mechanisms: the DMM model mainly involved increasing vessel invasion while the aged model involved both vessel invasion and tissue thinning.

The present study provides information regarding transport barriers and conduits for molecular exchange in normal and OA joints. We first tested the permeability of the major structural barrier (i.e., the calcified cartilage matrix and the osteochondral interface) to transport of biochemical signals using a FLIP approach. FLIP has been successfully applied to transport quantification across normal joints [10], with the FLIP technique providing the distinct advantage of a higher sensitivity to low permeability situations when compared with traditional tracer desorption or fluorescence recovery after photobleaching methods. We found a 31–37% and 0–42% reduction (although not statistically significant) in the permeability of the calcified cartilage and the osteochondral interface(C-C and O-C measures) that resulted from 8 weeks of altered joint loading or aging, respectively. Thus the ECM in the two OA models became more restrictive for diffusion of our small testing molecules (376Da fluorescein), possible due to hypermineralization of the ECM that is typically seen in OA [14–17]. Since in vivo signaling molecules are usually proteins with larger molecular weights than our testing molecules, their passage through the ECM of OA joints would presumably be even more restricted.

Interestingly, increasing numbers of large transport conduits (vascular channels or marrow cavities) were found to break the osteochondral interface and to advance towards the tidemark in the OA joints (Fig. 1 and Table 2). The presence of these large perforating channels greatly increases the overall transport capacity across the joint, overcoming the transport barriers posed by the denser ECM. Unlike the small nanopores found in the calcified matrix [10], these large conduits are expected to facilitate the transport of large signaling molecules due to their large pore sizes (on the order of 10-microns). Based on the average number density of the invading vessels, one can readily estimate the spacing of the vascular channels in the calcified cartilage to be 81, 55, and 67 μm for the control, aged, and DMM groups, respectively. Assuming the diffusivity of sodium fluorescein in these channels is close to free diffusion (532 $\mu m^2/s$) [24], the effective diffusivity of the tracer in the tissue cylinder surrounding the invading vessel is expected to scale with the square of the ratio of the vessel dimension (~10 μm in diameter) over that of the tissue cylinder (i.e., vessel spacing). The effective diffusivity is thus estimated to be 8 $\mu m^2/s$ (for the normal joints), and increased to 18 and 12 $\mu m^2/s$ for the aged and DMM joints, respectively. Furthermore, a fraction of vessels that penetrated all the way through the calcified cartilage were found to breach the tidemark every 160 or 236 μm in the aged and DMM joints, respectively. These vessels provided the most efficient pathway for direct molecular transport between subchondral bone and articular cartilage. This cross-talk capacity is anticipated to be even more elevated for the aged joints after considering the significant thinning of the calcified tissue layers (Fig. 4 of the present study and reference [28]). Our results were consistent with the conductance measurements performed on OA osteochondral samples [29].

In the present study, we tested two OA models; one induced by ageing and the other by altered joint loading, two major risk factors for OA [1]. The two models exhibited mild cartilage damage in our hands (average score on the order of 1.2 out of a full range of 6), which was consistent with previous studies [23, 30]. These mild OA models provided opportunities to study tissue alterations associated with the early stage(s) of OA. While not statistically significant tissue permeabilities in the two OA models were reduced compared to that of the normal age control. This lack of statistical significance among the groups may be due to the small sample sizes used in the study (n=4–5) and the relatively large variation in the data (coefficient of variation in the range of 20–50%, Table 1). Heterogeneous tissue local mineralization may be a possible factor for the data scattering [14], as well as errors associated with fluorescence imaging and curve fitting. Larger sample size will be needed to account for the large data variance in future studies. Consistent with previous reports [18, 19], increased vessel invasion was detected in both OA models with some vessel approaching (and occasionally breaching) the tidemark. The molecular mechanisms for this directed vessel growth process remains unclear. We speculate that pro-angiogenic factors may be involved in our OA models and a potential source for these factors is the hypertrophic chondrocytes [31, 32]. Whether angiogenesis directly influence the loss of cartilage matrix in vivo, as suggested in an in vitro grafting study [33], needs to be tested in future studies. However, we do know from the present study that the communication capacity between bone and cartilage is greatly increased in the two OA models through slightly different mechanisms. Increased cross-talk was achieved mainly by vessel invasion and thinning of the transport barrier (calcified tissues) in aged joints, whereas only vessel invasion is increased in the altered loading OA model two months post surgery. Whether tissue thinning would occur during later time points in DMM animals needs to be tested further.

One limitation of this study was that we did not track physiological signaling molecules involved in the OA development. Instead we used a fluorescent marker as a surrogate for the convenience of imaging. However, the diffusivity and effective transport pathway data

obtained herein could be readily extrapolated to small nutrients and small bioactive molecules. Let's consider the scenario where prostaglandin E2 and nitric oxide (with similar molecular weight as sodium fluorescein) are released in the subchondral bone regions during bone turnover [34]. Assuming the diffusivity of fluorescein, they could readily permeate the calcified cartilage over a distance of 58 μm within half an hour (i.e., $\sqrt{[4Dt]}=58$ μm, for $D=0.48$ $\mu m^2/s$ and $t=0.5$ h). If a capillary penetrated the joints as occurred in the aged and DMM joints, the signaling molecules could cover the same distance within a matter of seconds. These surprisingly fast transport processes may contribute to the elevated concentrations in the OA joints, providing an alternative explanation of the sources of these molecules in the in vivo studies, where inhibition of these molecules provided beneficial effects on cartilage [35, 36]. The second limitation was that the current study did not address the mechanistic questions such as the direction of the bone-cartilage cross-talk (signaling) and the nature of soluble signals. Due to the large surface area of cartilage and the presence of transport barriers (calcified cartilage and osteochondral interface), surface-down signaling mechanisms are appealing in studying OA pathology. Such mechanisms are well-accepted for a related cartilage degenerative disease, rheumatoid arthritis. However, early changes observed in OA patients typically involve the bone compartment [4–6], and inhibition of bone remodeling arrested the progression of OA in animal studies [7]. These lines of evidence lead to the hypothesis that signaling from bone to cartilage (bottom-up mechanisms) may lead to OA development [3]. Our results demonstrated increased transport potential in OA joints, but they do not support or exclude either surface-down or bottom-up cross-talk. More specifically designed experiments are needed to resolve this question. We speculate that the likely candidates for the bone-cartilage cross-talk signaling molecules may include bone remodeling byproducts (such as transform growth factor-beta, insulin-like growth factors, and fibroblast growth factors), and osteoclast and osteoblast activation factors (such as nitric oxide, prostaglandin E2, and receptor activator of nuclear factor kappa-B ligand) derived from cells in marrow, bone, or cartilage. In vitro co-culture and targeted blocking studies may help identify the signaling molecules. Lastly, the current study did not answer whether bone-cartilage cross-talk is the cause or result of OA development. We are currently investigating whether inhibition of bone turnover and angiogenesis would prevent or delay OA development after DMM surgery. More studies are needed to fully elucidate the role of bone in OA. If confirmed, bone may provide an effective pharmaceutical target for OA treatment.

Conclusions

this investigation provided quantitative measurements of transport characteristics of the joints from the aged, surgically destabilized, and normal age control mice. Elevated molecular transport was found in the OA joints, and various mechanisms (altered local matrix permeability, vessel invasion, and thinning of the transport resistant layers) were identified. Our data support further studies on subchondral bone, its role in OA development, and potential for OA treatments.

Acknowledgments

We thank Dr. Sonya Glasson for demonstrating the DMM surgery, Dr. Weidong (William) Yang for initiating the DMM operations, Mr. Frank Warren for animal care, and Dr. Chaoying Ni for providing the cryostat. Author contributions are the following: hypothesis formulation (LW), experimental design (LW, JP), microsurgery (WL), data collection (JP, BW,TS, YY, and CP), data analysis (JP, BW, ZZ, CP, and LW), data interpretation (LW, JP, and CP), and manuscript preparation and revision (LW, JP, CP, and BW). This study was supported by grants from NIH of US (P20RR016458; R01AR054385 to LW) and from China (NSF10972243 to JP and China Council Fellowship to BW).

References

1. Buckwalter JA, Martin JA. Osteoarthritis. Adv Drug Deliv Rev. 2006; 58(2):150–67. [PubMed: 16530881]
2. Goldring MB, Goldring SR. Articular cartilage and subchondral bone in the pathogenesis of osteoarthritis. Ann N Y Acad Sci. 2010; 1192:230–7. [PubMed: 20392241]
3. Lories RJ, Luyten FP. The bone-cartilage unit in osteoarthritis. Nat Rev Rheumatol. 2011; 7(1):43–9. [PubMed: 21135881]
4. Imhof H, et al. Degenerative joint disease: cartilage or vascular disease? Skeletal Radiol. 1997; 26(7):398–403. [PubMed: 9259096]
5. Kwan Tat S, Lajeunesse D, Pelletier JP, Martel-Pelletier J. Targeting subchondral bone for treating osteoarthritis: what is the evidence? Best Pract Res Clin Rheumatol. 2010; 24:51–70. [PubMed: 20129200]
6. Lajeunesse D. The role of bone in the treatment of osteoarthritis. Osteoarthritis Cartilage. 2004; 12(Suppl A):S34–8. [PubMed: 14698639]
7. Kadri A, et al. Osteoprotegerin inhibits cartilage degradation through an effect on trabecular bone in murine experimental osteoarthritis. Arthritis Rheum. 2008; 58(8):2379–86. [PubMed: 18668550]
8. Botter SM, et al. ADAMTS5-/- mice have less subchondral bone changes after induction of osteoarthritis through surgical instability: implications for a link between cartilage and subchondral bone changes. Osteoarthritis Cartilage. 2009; 17(5):636–45. [PubMed: 19010693]
9. Sanchez C, et al. Subchondral bone osteoblasts induce phenotypic changes in human osteoarthritic chondrocytes. Osteoarthritis Cartilage. 2005; 13(11):988–97. [PubMed: 16168681]
10. Pan J, et al. In situ measurement of transport between subchondral bone and articular cartilage. J Orthop Res. 2009; 27(10):1347–52. [PubMed: 19360842]
11. Hodge JA, McKibbin B. The nutrition of mature and immature cartilage in rabbits. An autoradiographic study. J Bone Joint Surg Br. 1969; 51(1):140–7. [PubMed: 5766355]
12. Honner R, Thompson RC. The nutritional pathways of articular cartilage. An autoradiographic study in rabbits using 35S injected intravenously. J Bone Joint Surg Am. 1971; 53(4):742–8. [PubMed: 5580031]
13. Ogata K, Whiteside LA. Barrier to material transfer at the bone-cartilage interface: measurement with hydrogen gas in vivo. Clin Orthop Relat Res. 1979; (145):273–6. [PubMed: 535282]
14. Ferguson VL, Bushby AJ, Boyde A. Nanomechanical properties and mineral concentration in articular calcified cartilage and subchondral bone. J Anat. 2003; 203(2):191–202. [PubMed: 12924819]
15. Imhof H, et al. Importance of subchondral bone to articular cartilage in health and disease. Top Magn Reson Imaging. 1999; 10(3):180–192. [PubMed: 10565710]
16. Miller LM, et al. Alterations in mineral composition observed in osteoarthritic joints of cynomolgus monkeys. Bone. 2004; 35(2):498–506. [PubMed: 15268902]
17. Radin EL, Rose RM. Role of subchondral bone in the initiation and progression of cartilage damage. Clin Orthop Relat Res. 1986; (213):34–40. [PubMed: 3780104]
18. Clark JM. The structure of vascular channels in the subchondral plate. J Anat. 1990; 171:105–15. [PubMed: 2081697]
19. Imhof H, et al. Subchondral bone and cartilage disease: a rediscovered functional unit. Invest Radiol. 2000; 35(10):581–8. [PubMed: 11041152]
20. Burr DB, Schaffler MB. The involvement of subchondral mineralized tissues in osteoarthrosis: quantitative microscopic evidence. Microsc Res Tech. 1997; 37(4):343–57. [PubMed: 9185156]
21. Burr DB, Radin EL. Microfractures and microcracks in subchondral bone: are they relevant to osteoarthrosis? Rheum Dis Clin North Am. 2003; 29(4):675–85. [PubMed: 14603577]
22. Bendele AM. Animal models of osteoarthritis. J Musculoskelet Neuronal Interact. 2001; 1(4):363–76. [PubMed: 15758487]
23. Glasson SS, Blanchet TJ, Morris EA. The surgical destabilization of the medial meniscus (DMM) model of osteoarthritis in the 129/SvEv mouse. Osteoarthritis Cartilage. 2007; 15(9):1061–9. [PubMed: 17470400]

24. Wang L, et al. In situ measurement of solute transport in the bone lacunar-canalicular system. Proc Natl Acad Sci U S A. 2005; 102(33):11911–6. [PubMed: 16087872]
25. Leddy HA, Guilak F. Site-specific molecular diffusion in articular cartilage measured using fluorescence recovery after photobleaching. Ann Biomed Eng. 2003; 31(7):753–60. [PubMed: 12971608]
26. Burr DB, Hooser M. Alterations to the en bloc basic fuchsin staining protocol for the demonstration of microdamage produced in vivo. Bone. 1995; 17(4):431–3. [PubMed: 8573418]
27. Lajeunesse D, Reboul P. Subchondral bone in osteoarthritis: a biologic link with articular cartilage leading to abnormal remodeling. Curr Opin Rheumatol. 2003; 15(5):628–33. [PubMed: 12960492]
28. Lane LB, Bullough PG. Age-related changes in the thickness of the calcified zone and the number of tidemarks in adult human articular cartilage. J Bone Joint Surg Br. 1980; 62(3):372–5. [PubMed: 7410471]
29. Hwang J, et al. Increased hydraulic conductance of human articular cartilage and subchondral bone plate with progression of osteoarthritis. Arthritis Rheum. 2008; 58(12):3831–42. [PubMed: 19035476]
30. Dieppe P, et al. Prediction of the progression of joint space narrowing in osteoarthritis of the knee by bone scintigraphy. Ann Rheum Dis. 1993; 52(8):557–63. [PubMed: 8215615]
31. Ashraf S, Walsh DA. Angiogenesis in osteoarthritis. Curr Opin Rheumatol. 2008; 20(5):573–80. [PubMed: 18698180]
32. Pesesse L, Sanchez C, Henrotin Y. Osteochondral plate angiogenesis: a new treatment target in osteoarthritis. Joint Bone Spine. 2011; 78(2):144–9. [PubMed: 20851653]
33. Fenwick SA, Gregg PJ, Rooney P. Osteoarthritic cartilage loses its ability to remain avascular. Osteoarthritis Cartilage. 1999; 7(5):441–52. [PubMed: 10489316]
34. Burr DB. Increased biological activity of subchondral mineralized tissues underlies the progressive deterioration of articular cartilage in osteoarthritis. J Rheumatol. 2005; 32(6):1156–8. discussion 1158–9. [PubMed: 15977355]
35. Chabane N, et al. Histone deacetylase inhibitors suppress interleukin-1beta-induced nitric oxide and prostaglandin E2 production in human chondrocytes. Osteoarthritis Cartilage. 2008; 16(10): 1267–74. [PubMed: 18417374]
36. Studer R, et al. Nitric oxide in osteoarthritis. Osteoarthritis Cartilage. 1999; 7(4):377–9. [PubMed: 10419772]

Highlights

- Elevated bone-cartilage cross-talk was hypothesized in altered loading (DMM) and ageing induced OA joints
- Decreased (but not significant) tissue permeability in mineralized ECM in OA joints
- Increased number of blood vessels invading calcified cartilage in aged (+100%) and DMM (+50%) joints vs. controls
- 60% thinning of the subchondral bone and calcified cartilage layers in aged joints and no changes of tissue layer thickness in DMM joints
- Overall bone-cartilage cross-talk capacity elevated in the two OA models through different mechanisms

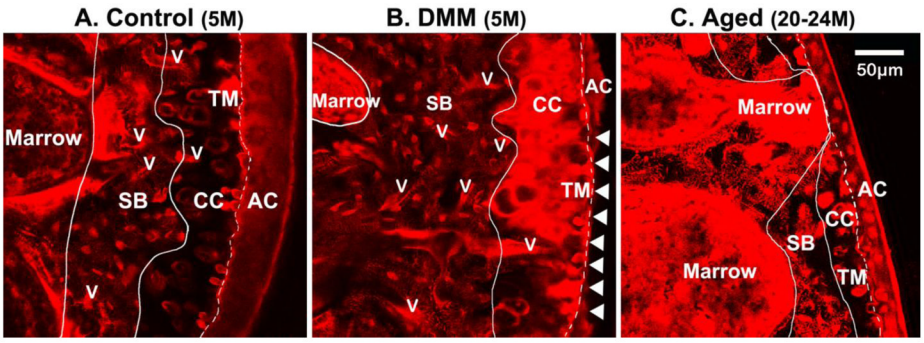

Figure 1.

Invading vessels and tissue layers in murine distal femurs from (A) normal 5-month-old mice (Control), (B) DMM mice (5-month-old, 8 week post surgery), and (C) aged 20–24-month-old mice. The slices are captured using z-stack confocal imaging of the plastic embedded femoral epiphysis bulk stained with basic fuchsin. Visualized in the 3D confocal z-stacks, the articular cartilage (AC), calcified cartilage (CC), tidemark (TM), and subchondral bone (SB) can be readily identified due to distinct cell morphology and tissue staining patterns as shown here. Invading vessels (v) and marrow cavities were clearly visualized and traced within the 3D image stacks. Compared with the younger normal control joint where invading vessels are mostly located in SB (panel A), increasing incidence of vascular channel penetrating into CC and even contacting TM can be seen in the DMM and aged joints (panels B and C, respectively). Articular cartilage erosions indicated with arrow heads can be found in the DMM sample shown in Panel B, and thinning of the AC, CC, and SB layers is obvious in this aged sample shown in Panel C.

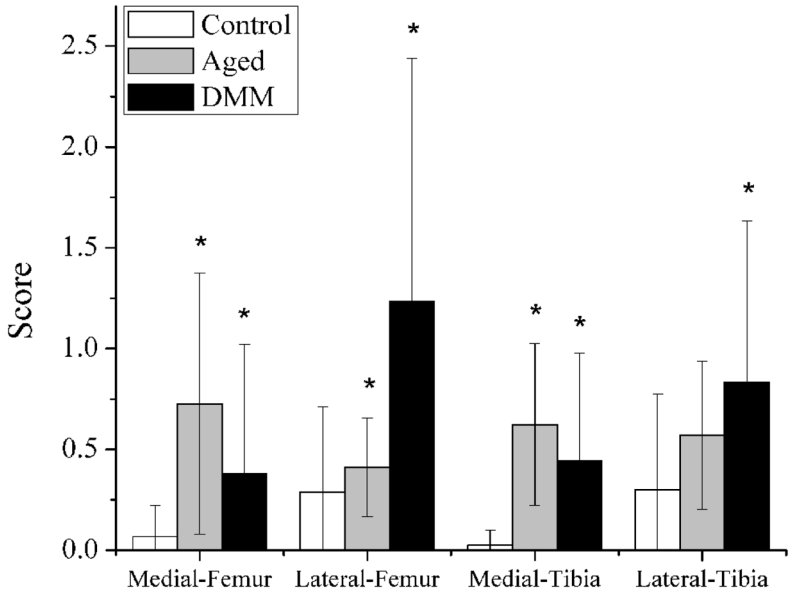

Figure 2.

Validation of the two OA models. The histological scores of cartilage damage were obtained within the four quadrants of the right knees from the aged (20–24-month-old), DMM (5-month-old), and control mice (5-month-old). Compared with the normal age controls, higher average scores were seen in most quadrants of the aged joints (except for lateral tibia) and in all four quadrants of the DMM joints 8 weeks post surgery (indicates $p < 0.05$ vs. controls). Overall, the damage was mild (average OA score less than 1.2 out of a full range of 6) for both the aged and the DMM joints.

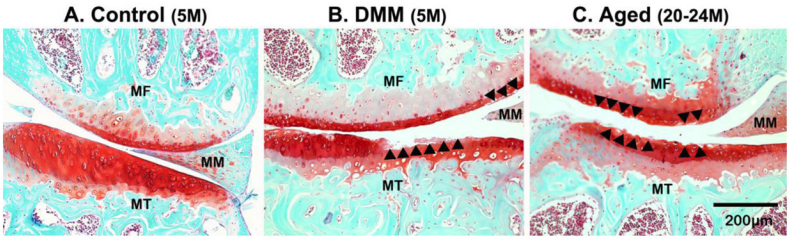

Figure 3.

Selected Safranin-O/Fast Green stained sections are shown for (A) control, (B) DMM, and (C) aged knee joints. Smooth articular surface was seen in the medial femoral condyle (MF) and medial tibial plateau (MT) from a 5-month-old control mouse (Panel A); damage areas indicated with arrowheads were found in the DMM (Panel B) and the aged joint (Panel C).

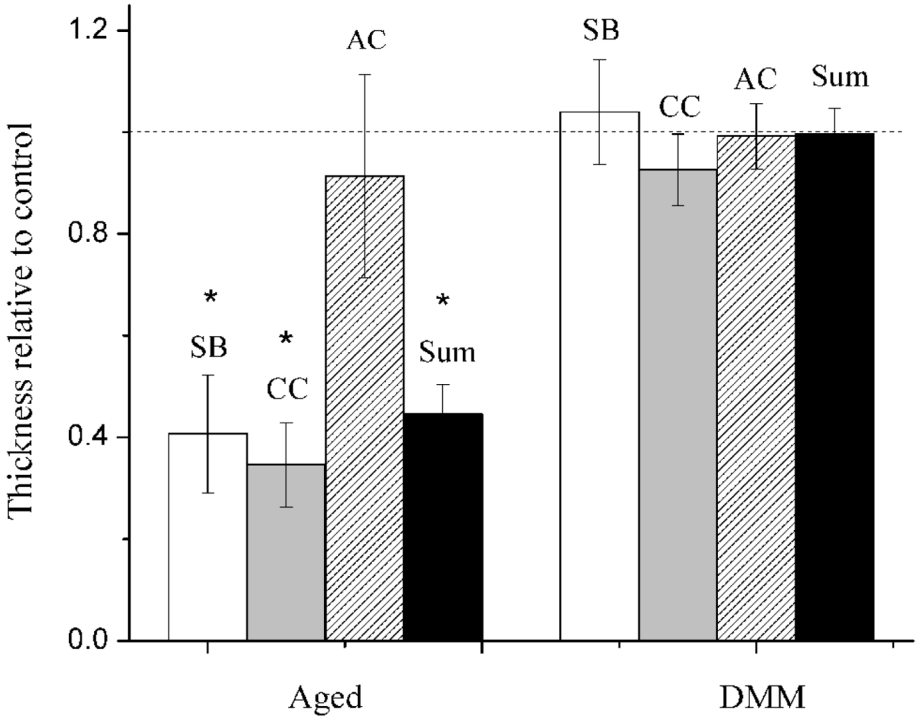

Figure 4.
Thickness of the subchondral bone (SB), calcified cartilage (CC), articular cartilage (AC), and the total thickness (the sum of SB, CC, and AC) of the distal femoral epiphysis in the aged and DMM OA joints. The data were normalized with the normal age controls. * indicates $p<0.05$ vs. controls using Student-t tests.

Table 1

The matrix permeability measured using sodium fluorescein in the murine knee joints

Group (joint side, sample size)	Age	Diffusivity ($\mu m^2/s$) C-C (mean±SD)	Diffusivity ($\mu m^2/s$) O-C (mean±SD)
DMM (right knees, n=5)	5 months	0.30±0.17	0.12±0.04
Control (DMM left knees, n=5)	5 months	0.48±0.13 *	0.12±0.06 *
Aged (right knees, n=4)	20–24 months	0.33±0.20	0.07±0.03

Keys:

SD = standard deviation

C-C = measurements in calcified cartilage between chondrons;

O-C = measurements across the osteochondral interface between osteocyte and chondron;

n = number of joints per group

* $p < 0.05$, two-tailed paired Student t test between C-C and O-C measures of the Control group;

Table 2

The number density of invading vessels in the right distal femoral epiphyses

Group (sample size)	Age	Number density of invading vessels (#/mm^2)		
		SB (mean + SD)	CC (mean + SD)	TM (mean + SD)
DMM (n=4)	5 months	427.9±110.8	222.4±72.6	18.1±15.8
Control (n=4)	5 months	327.1±178.0	151.5±139.3	0
Aged (n=4)	20–24 months	209.5±113.5	332.2±86.4	51.3±40.6 *

Keys:

SD = standard deviation

SB = subchondral bone;

CC = calcified cartilage;

TM = tidemark

* $p < 0.05$, two-tailed Student t-test (Aged vs. Control)